CHEMISTRY OF MATERIALS

pubs.acs.org/cm

Article

Uniform Supported Metal Nanocrystal Catalysts Prepared by Slurry Freeze-Drying

Andy Y. Yang and Matt Law*

Cite This: https://dx.doi.org/10.1021/acs.chemmater.0c03615

Read Online

ACCESS | Metrics & More | Article Recommendations | Supporting Information

ABSTRACT: Colloid immobilization is an established way to load metal nanocrystals (NCs) onto solid supports to make heterogeneous (photo)-catalysts. The use of preformed colloidal NCs enables excellent control of NC composition, size, and shape compared to alternative catalyst preparation methods, but this approach often suffers from uncontrolled NC aggregation, nonuniform NC loading, and strongly bound ligands on the NC surface that inhibit catalytic activity. Here, we show that freeze-drying of aqueous slurries of gold NCs and various powdered supports (cellulose, TiO_2, Al_2O_3, SiO_2, carbon) produces highly uniform, well-dispersed supported NCs over a wide range of NC loadings (to at least 20 wt %) and batch sizes (to at least 1 g). Rinsing supported citrate-capped NCs with water removes citrate ligands to yield active gold surfaces without the need for high-temperature calcination. The reduction of Pt^{4+} to Pt^0 and 4-nitrophenol to 4-aminophenol on the surface of the supported NCs is used to demonstrate the activity of these catalysts. Slurry freeze-drying offers superior product uniformity, reproducibility, and scalability and should prove useful as a simple and general method for making supported NC catalysts, including plasmonic photocatalysts.

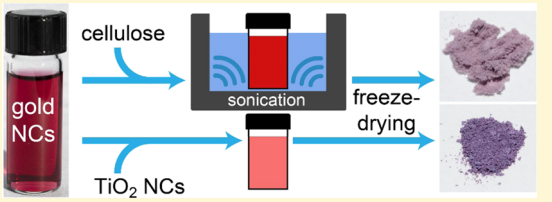

INTRODUCTION

Metal nanocrystals (NCs) supported on high-surface-area solids are an important class of heterogeneous catalysts.[1−5] Supported metal NCs are made by either growing NCs directly on a support (often by liquid-phase metal salt deposition and reduction) or immobilizing preformed colloidal NCs on a support. Direct NC growth methods (salt deposition,[6] coprecipitation,[7] deposition−precipitation,[8,9] ion exchange, chemical vapor deposition, cosputtering, etc.) can yield metal NCs with clean surfaces and interfaces, but control of NC size, shape, and coverage on the support is usually poor and NC polydispersity, clustering, and coverage nonuniformity are common problems.[2,3,10−12] In contrast, the deposition of preformed, highly monodisperse colloidal NCs offers excellent control of NC size and shape, but depositing colloidal NCs uniformly throughout a support is challenging because (i) NC binding to the support is often too weak or too strong and difficult to control[13−18] and (ii) when NCs are weakly bound to the support, conventional drying allows motion of the solvent, NCs, and support particles that results in NC/support unmixing and nonuniform NC loading.[1,2,19−21] In addition, the ligands used in NC synthesis tend to inhibit catalyst activity and decrease stability.[21,22] Attempts to clean the NC surface by exchanging or removing the ligands with chemical or thermal treatments usually degrade the NC monodispersity,[1,12,13,17,18,21,23−25] although size/shape changes can be suppressed if the NCs are encapsulated within nanostructured materials such as mesoporous silica.[26−29]

The advent of a general, scalable approach to uniformly load colloidal NCs onto solid supports while preserving NC size and shape would be valuable for the development of improved catalysts. This is particularly true for plasmonic photocatalysts,[30] whose optical absorption spectra and local electromagnetic field enhancements depend sensitively on NC size, shape, and coupling with other NCs and the support. To avoid contamination that can reduce catalyst activity and stability, the new approach should employ purified NCs and achieve uniform, tunable NC loading without the need for additives to promote NC-support binding.[21,31−34]

Freeze-drying (lyophilization) offers a way to make uniform supported NCs by avoiding the need to adsorb NCs from a liquid onto a support and preventing unmixing of NCs and support during drying. Freeze-drying employs rapid freezing at low temperature followed by in vacuo sublimation of water to gently produce dehydrated solids. It is a mature technology common in many sectors, most notably the food and pharmaceutical industries.[35] Freeze-drying has been used to dry colloidal NC dispersions to prepare reconstitutable NC powders for improved storage, transport, and shelf life.[36−41] In addition to NC powders, freeze-drying has been utilized to make supported metal NC catalysts by mixing a support material with a dissolved or molten metal salt, freeze-drying the

Received: September 9, 2020
Revised: December 10, 2020

mixture, and then reducing the metal salt at high temperature to grow metal NCs on the support.[42−46] Kim et al. modified this process by chemically reducing the metal salt while it stirred with the support, then filtering, washing, and freeze-drying the resulting solid.[47,48] The application of freeze-drying in these direct NC growth methods generally improves the uniformity of NC loading, but the NC size and shape distributions remain broad and uncontrolled. By employing monodisperse colloidal NCs instead of metal salts, it should be possible to use freeze-drying to produce uniform supported NC catalysts with excellent control of NC size and shape.

Here, we show that freeze-drying of aqueous slurries of gold (Au) NCs and a powdered support (cellulose, TiO_2, Al_2O_3, SiO_2, carbon) yields highly uniform supported Au NC catalysts with retention of the original NC monodispersity. This freeze-drying process is effective for a range of NC loadings (to at least 20 wt %) and batch sizes (to at least 1 g). Using NCs with a weakly bound ligand that readily desorbs in water (citrate), we eliminate the calcination step that is normally needed to activate catalysts prepared by NC deposition. The resulting solids are demonstrated to be catalytically active for solution-phase reductive platinum deposition and reduction of 4-nitrophenol to 4-aminophenol. The applicability of the process to different types of NCs is illustrated by preparing gold triangular nanoprisms supported on cellulose and TiO_2. Our work shows that slurry freeze-drying is a simple, reproducible, general, and scalable method to make uniform and active supported NC catalysts from monodisperse colloidal NCs.

EXPERIMENTAL METHODS

Chemicals. All chemicals were used as received unless otherwise noted. 18.2 MΩ water (Millipore Milli-Q Gradient) was used throughout the study. Hydrogen tetrachloroaurate(III) trihydrate ($HAuCl_4{\cdot}3H_2O$, 99.99%) and potassium iodide (KI, 99.9%) were purchased from Alfa Aesar. Trisodium citrate dihydrate (>99.8%) was purchased from MP Biomedical. Microcrystalline cellulose (MCC; 90 μm average particle size), titanium(IV) oxide (Aeroxide P25), and sodium borohydride ($NaBH_4$, 99%) were purchased from Acros. Cetyltrimethylammonium chloride solution (CTAC, 25 wt % in H_2O), 4-nitrophenol (≥99%), aluminum(III) oxide nanopowder (γ-Al_2O_3, <50 nm), and hexachloroplatinic(IV) acid hydrate ($H_2PtCl_6{\cdot}xH_2O$, ≥ 99.9%) were purchased from Sigma-Aldrich. Silicon dioxide (SiO_2) nanopowder (US3435, 98%+, 60−70 nm diameter) and activated carbon nanopowder (US1078, >95%, <100 nm diameter) were purchased from U.S. Research Nanomaterials. L-Ascorbic acid and methanol (99.9%) were purchased from Fisher Scientific. Sodium bicarbonate 99.7% (7412-06) and nitric acid 68% (2704-14) were purchased from Macron Fine Chemicals.

Synthesis of Spheroidal Au Nanocrystals. A modified citrate reduction method[49] was used to synthesize spheroidal Au NCs of 12−14 nm diameter. One hundred thirty milligrams of trisodium citrate dihydrate was dissolved in 200 mL of water and heated to boiling on a hot plate with moderate stirring. Four milliliters of 25 mM aqueous $HAuCl_4$ was then quickly added to this solution and, after 20 min of stirring, the resulting dark red NC dispersion was cooled in an ice bath. The NCs were purified by dialysis filtration using Amicon Ultra-15 Centrifugal Filter Units (UFC905024, 50 kDa cutoff)[50] to remove solutes and loosely bound ligands (i.e., citrate, NaCl, and other byproducts) without subjecting the NCs to precipitation and redispersion cycling that can cause incomplete NC recovery and an altered size distribution. Briefly, 12.5 mL aliquots of the reaction mixture were centrifuge filtered at 3000 rcf for 3 min and the resulting concentrated colloidal retentate (<1 mL volume) was rediluted to 12.5 mL with water. Each aliquot was filtered again, diluted again, and filtered a third time to give a >2000-fold reduction in solute concentrations with no loss of NCs. The purified aliquots were then combined and diluted with water to a total volume of 20 mL (final NC concentration of ∼1 mg/mL).

Synthesis of Triangular Au Nanoprisms. We used the seeded growth and purification method of Scarabelli et al. to synthesize triangular Au nanoprisms.[51] Spheroidal Au NC seeds were prepared by mixing 50 μL of 25 mM aqueous $HAuCl_4$ with 4.7 mL of 100 mM aqueous CTAC in a 20 mL scintillation vial at room temperature, and then injecting 100 μL of a freshly made, ice-cold 30 mM $NaBH_4$ solution under vigorous stirring. The seed dispersion was stirred continuously for 2 h, then diluted 10-fold with a 100 mM CTAC solution. To grow the seeds into larger NCs, 200 μL of the seed dispersion was added to a vial containing 80 μL of 25 mM $HAuCl_4$, 1.6 mL of 100 mM CTAC, 15 μL of 10 mM KI, 40 μL of 100 mM ascorbic acid, and 8 mL of water and shaken for 1 s. To grow large NCs into triangular nanoprisms of 55−60 nm edge length, 3.2 mL of this colloid was immediately transferred to a 50 mL flask containing 1 mL of 25 mM $HAuCl_4$, 2.86 mL of 25% CTAC, 0.3 mL of 10 mM KI, 400 μL of 100 mM ascorbic acid, and 37.14 mL of water and shaken for several seconds. The flask was left undisturbed for 1 h at ambient conditions, resulting in a mixed dispersion of nanoprisms and spheroidal NCs. The nanoprisms were selectively flocculated by adding 10 mL of 25% CTAC and allowed to precipitate overnight (16 h) in a conical-bottom centrifuge tube. The supernatant was removed and the precipitate redispersed in 20 mL of water, yielding a bright blue dispersion of nanoprisms. In contrast to the NCs, the nanoprisms were not further purified by diafiltration because the centrifuge filters were clogged by CTAC.

Preparation of Supported NCs. NCs supported on MCC were prepared by adding 0−9 mL of water to 100 mg of MCC powder in a vial, then injecting 0−5 mL of 50 mM aqueous trisodium citrate followed by 1−10 mL of the Au NC dispersion (1 mg/mL NCs), producing a series of slurries with 1, 2, 5, and 10 wt % NCs and 0−25 mM citrate at a total volume of 10 mL. Samples with 20 wt % NC loading were made by adding 50 mg of MCC to 10 mL of the NCs. Each slurry was sonicated for 60 min, briefly shaken for 2 s to homogenize the slurry, frozen at −78 °C in crushed dry ice for at least 30 min, and then freeze-dried in a homebuilt lyophilizer (20 mTorr base pressure) until completely dry (∼48 h). The resulting solids were pink to deep maroon in color (depending on the NC and citrate concentrations) with a spongelike texture. The Brunauer−Emmett−Teller (BET) surface area of the sonicated and freeze-dried MCC (without Au NCs) was measured by nitrogen gas adsorption to be 7 m^2/g.

TiO_2-supported and Al_2O_3-supported NCs with 1 and 5 wt % NCs were made in a similar fashion by mixing 100 mg of P25 TiO_2 or Al_2O_3 nanocrystals in 0−9 mL of water and adding 0−5 mL of 50 mM aqueous trisodium citrate followed by 1−5 mL of Au NCs for a total volume of 10 mL. The mixtures were shaken to form homogeneous slurries, as sonication was not needed to disperse the TiO_2 and Al_2O_3 nanopowders. The final freeze-dried products were fine to coarse powders with a violet to deep maroon color (depending on the NC and citrate concentrations). The BET surface area of the freeze-dried TiO_2 (without Au NCs or citrate) was measured by nitrogen gas adsorption to be 51 m^2/g. SiO_2-supported NCs (1% NCs) were prepared using an identical procedure.

To prepare carbon-supported NCs (1% NCs), 1 g of carbon nanopowder was added to 20 mL of 8 M aqueous HNO_3 in a scintillation vial. The mixture was briefly shaken and aged at room temperature for 90 min. The slurry was then neutralized with excess sodium bicarbonate, vacuum filtered, washed with water, and dried in an oven at 100 °C for 1 h. Next, a NC/support slurry was made by mixing 100 mg of the support, 9 mL of water, and 1 mL of the 1 mg/mL NC dispersion. The slurry was freeze-dried as described above.

Preparation of Supported Nanoprisms. Nanoprisms supported on MCC were prepared by adding 100 mg of sonicated and freeze-dried MCC powder to 10 mL of the nanoprism dispersion. This slurry was shaken to suspend the cellulose particles, frozen in crushed dry ice for at least 30 min, and then freeze-dried as described above. Sonication of the slurry was avoided to prevent possible changes to the shape of the nanoprisms. The product was a fine

https://dx.doi.org/10.1021/acs.chemmater.0c03615
Chem. Mater. XXXX, XXX, XXX−XXX

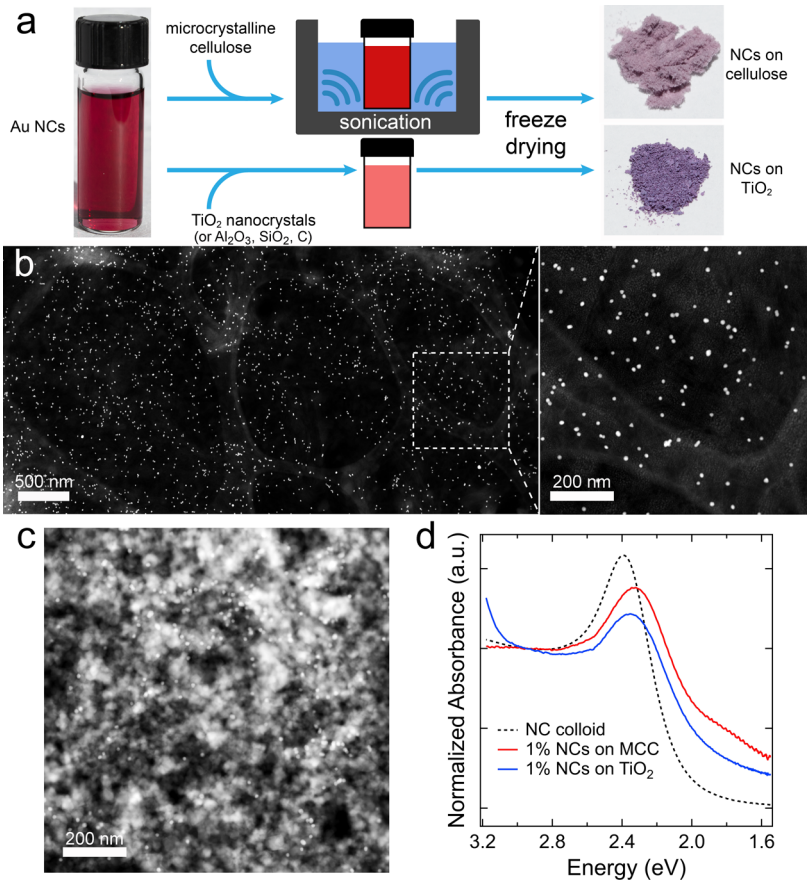

Figure 1. Preparation of well-dispersed gold NCs on high-surface-area solid supports by freeze-drying. (a) Process flow. Purified gold NCs in water are mixed with a powder of the support (microcrystalline cellulose, TiO_2 or Al_2O_3 nanocrystals, or SiO_2 or carbon nanoparticles), sonicated (for cellulose only) and shaken, and then freeze-dried to yield a porous, high-surface-area solid uniformly loaded with well-dispersed NCs. (b) Low-magnification dark-field STEM image of 1 wt % Au NCs on MCC prepared without added citrate. This image shows a particularly flat region of the sample so that all of the NCs are in focus. At right is a magnified view of the region outlined in the dashed box. (c) Dark-field STEM image of 1 wt % NCs on nanocrystalline TiO_2, also prepared without added citrate. The small whitish spheroids are the NCs. (d) Optical absorbance spectra of dried layers of these NC/MCC and NC/TiO_2 samples. A spectrum of the aqueous dispersion of the NCs is shown for comparison. All spectra are normalized at λ = 420 nm ($h\nu$ = 2.95 eV).

powder light blue in color. TiO_2-supported nanoprisms were prepared similarly, using 100 mg of P25 TiO_2 powder and 10 mL of the nanoprism dispersion. The final freeze-dried product was a fine powder with a vivid light blue color. No citrate was added to either nanoprism slurry.

Material Characterization. Transmission electron microscopy (TEM) was performed on JEOL JEM-2100 and JEOL JEM-2800 TEMs at accelerating voltages of 200 kV. Samples were prepared by drop casting and drying 5 μL of the supported nanocrystal/nanoprism suspension on a standard TEM grid (#01824, Ted Pella) in air. Samples for optical extinction spectra were made by sandwiching 100 μL of supported nanocrystal/nanoprism suspension between two microscope cover slips and allowing the suspension to dry overnight. Optical transmittance (T) and reflectance (R) spectra (λ = 400–800 nm) were acquired on a PerkinElmer Lambda 950 spectrophotometer equipped with a 60 mm integrating sphere. Optical absorbance was calculated using the following equation: absorbance = $-\log(R + T)$. 4-Nitrophenol reduction experiments were carried out in 4.5 mL polystyrene cuvettes (759071D, BrandTech) in standard transmission geometry.

Attenuated total reflectance (ATR) Fourier transform infrared (FTIR) spectra were measured with a Nicolet 6700 FTIR spectrometer with GladiATR diamond ATR module (Pike Technologies) using 256 scans at 2 cm^{-1} resolution. The samples presented in Figure S1 were made by depositing 100 μL of the solution onto the ATR crystal and drying in a stream of nitrogen. The samples presented in Figure S15 were prepared by drop casting and drying 20 μL of a 20 mg/mL suspension of the supported NCs onto the ATR crystal. In situ water rinsing was performed by covering the sample with 20 μL of pure water, gently wicking the water away with a Kimwipe after 5 min, and allowing the sample to dry.

Thermogravimetric analysis (TGA) was performed on a TA Q500 TGA. Samples were placed on tared platinum pans and heated at a ramp rate of 20 °C/min from room temperature to 500 °C under constant nitrogen purge. Powder X-ray diffraction (XRD) was performed on a Rigaku SmartLab in Bragg–Brentano geometry using zero background plates. Samples were scanned from 10 to 60° with a step size of 0.05° at a scan rate of 6°/min. The surface area of the freeze-dried MCC and TiO_2 supports was measured with a Micromeritics 3Flex Surface Characterization Analyzer using nitrogen as the adsorption gas.

Thermal Reduction of Platinum on Supported Au NCs. Pt nanocrystals were deposited on MCC-supported Au NCs (5 wt %) by adding 40 mg of the supported NCs, 500 μL of 10 mM H_2PtCl_6, and 1 mL of methanol to 8.5 mL of water in a 25 mL two-neck round bottom flask fitted with a condenser. This mixture was degassed and refluxed at 65 °C for 6 h with constant argon purging and stirring. The resulting dark gray solid was collected by centrifugation and washed three times with water to remove residual Pt salts, byproducts, and methanol.

Reduction of 4-Nitrophenol to 4-Aminophenol. Reduction of 4-nitrophenol to 4-aminophenol on the surface of Au NCs was

https://dx.doi.org/10.1021/acs.chemmater.0c03615
Chem. Mater. XXXX, XXX, XXX–XXX

studied by in situ optical extinction spectroscopy in stirred cuvettes cooled to 15 °C with a recirculating bath (LT ecocool 150, Grant Instruments). Experiments were performed at both 1 and 5 wt % NC loadings. 1 mg/mL suspensions of the MCC- and TiO_2-supported NCs were prepared by adding 4 mg of the supported NC powder to 4 mL of water and stirring. In the 5 wt % tests, 1.0 mL of freshly made, ice cold 45 mM $NaBH_4$ and 60 μL of the supported NC suspension were added to 1.88 mL of water in a 4.5 mL cuvette and stirred for 5 min at 15 °C, at which time 60 μL of a 5 mM 4-nitrophenol solution was injected into the cuvette to initiate the reaction. The 1 wt % NC tests used 1.64 mL of water and 300 μL of the supported NC suspension. Control experiments with unsupported colloidal NCs were performed using 1.91 mL of water, 1.0 mL of 45 mM $NaBH_4$, 30 μL of a 100 μg/mL NC dispersion, and 60 μL of 5 mM 4-nitrophenol. Initial reactant and NC concentrations were the same in all cases (100 μM 4-nitrophenol, 15 mM $NaBH_4$, and 1 μg/mL NCs). Loss of 4-nitrophenolate was monitored by recording its absorption peak at λ = 400 nm under continuous temperature control and stirring.

RESULTS AND DISCUSSION

Figure 1a outlines the process used here to load preformed gold NCs onto solid supports. Spheroidal, citrate-capped Au NCs with a diameter of 12−14 nm were synthesized in water using a published method[49] and purified by centrifuge dialysis filtration, which removes molecular solutes without causing aggregation or loss of NCs (see the Experimental Methods section and Figure S1).[50,52,53] A known amount of a powdered support material (microcrystalline cellulose (MCC), TiO_2 nanocrystals, γ-Al_2O_3 nanocrystals, SiO_2 nanoparticles, or carbon nanopowder) was then added to the purified NC dispersion and the mixture shaken (for TiO_2, Al_2O_3, SiO_2, and carbon) or sonicated and then shaken (for MCC) to make a homogeneous slurry, frozen in dry ice at −78 °C, and freeze-dried in a homebuilt lyophilizer (Figure S2). MCC was selected for study because it is an insoluble, chemically robust, and low-cost organic support, while TiO_2, γ-Al_2O_3, SiO_2, and activated carbon are common inorganic supports. We found that sonication was necessary to form homogeneous MCC slurries by decreasing the MCC particle size, but sonication also partially amorphized the cellulose, which probably decreases its thermal and chemical stability (Figure S3). Sonication was not needed for the TiO_2, Al_2O_3, SiO_2, or carbon slurries because these supports formed stable suspensions upon brief shaking.

The resulting freeze-dried products are uniform in color and texture. For example, MCC and TiO_2 loaded with 1 wt % NCs and no added sodium citrate (*vide infra*) have a uniform pink and violet color, respectively, suggesting that the NCs are distributed homogeneously throughout both supports (Figure 1a). Scanning transmission electron microscopy (STEM) images confirm that the NCs are intact and well dispersed on both MCC and TiO_2 (Figures 1b,c and S4). A comparison of secondary electron and dark-field STEM images shows that the NCs are distributed over all of the solution-accessible surfaces of the support rather than being located only on the outer surface of the support agglomerates (Figures S4 and S5). The NC/MCC solids have a fluffy, spongelike texture, while the NC/TiO_2 solids are coarse, free-flowing powders. Slurry freeze-drying also yielded uniform loading of these NCs onto nanocrystalline γ-Al_2O_3 (Figure S6), SiO_2, and carbon supports (Figure S7), as well as ∼3.5 nm diameter citrate-capped NCs onto MCC and TiO_2 supports (Figure S7), further demonstrating the versatility of this method for loading NCs onto different supports.

In contrast to freeze-drying, conventional evaporative drying of the NC/MCC and NC/TiO_2 slurries resulted in inhomogeneous solids. Four methods of conventional drying were explored as control experiments. Evaporative drying at room temperature in unstirred open vials led to large vertical gradients in NC loading (more NCs near the top of the solids) as a consequence of the different suspendability limits and precipitation dynamics of the NCs and support material. This process was also irreproducible and very slow (4−5 weeks to evaporate 10 mL of water). Drying at 60 °C in a vacuum oven (no stirring) was faster (1 week) but gave similarly inhomogeneous products. We also investigated the use of rotary evaporation to dry the slurries. Rotary evaporation at 50 °C improved sample homogeneity compared to ambient and vacuum oven drying, but the directional drying inherent to rotary evaporation still resulted in a pronounced NC concentration gradient from the top to the bottom of the vials (more NCs near the bottom of the vials; Figure S8). Finally, we tested vacuum filtration as a way to collect and dry the slurries on nanoporous filters. We made a series of slurries (1 wt % NCs), thoroughly mixed them by brief shaking, and then filtered each within ∼1 min through a 0.2 μm nylon membrane filter using a Buchner funnel. This procedure resulted in uniformly colored retentates only for NC/TiO_2 slurries without added citrate. The other five types of slurries that we tested produced layered or otherwise inhomogeneous solids (Figure S9). The difficulty in obtaining uniform NC loading by these conventional drying methods shows that the NCs often have little tendency to adsorb to the support particles while stirred together as a slurry. To further test this notion, we stirred NC/TiO_2, NC/MCC, and NC/Al_2O_3 slurries continuously for 2 days at room temperature and then visually checked the extent of NC uptake by the support particles. We found complete NC uptake in only three of the six types of slurries tested, with the other three slurries showing little or no NC uptake (Figure S10). Although spontaneous NC adsorption by simple stirring of NC/support mixtures has been successfully used to make several types of supported NCs,[13−18] such adsorption occurs only for certain combinations of NCs, support, and solution composition (e.g., pH, ionic strength, ligands). By rapidly freezing well-mixed slurries and removing the frozen solvent by sublimation rather than evaporation, freeze-drying sidesteps the difficulties associated with NC adsorption from the liquid and prevents segregation of the NCs and support during drying, yielding more homogeneous products for a wider range of NC/support materials with less effort and time compared to conventional approaches.

Although often the NCs did not adsorb to the support particles while wet in the slurry, they always became strongly immobilized on the support once freeze-dried. Immersing the freeze-dried solids in water resulted in no visible leeching of NCs into the liquid. Furthermore, after resuspending the freeze-dried NC/MCC or NC/TiO_2 powders by shaking, the support particles retained their NCs as they slowly settled, leaving colorless supernatants free of NCs (Figure S11). We believe that a combination of electrostatic and van der Waals forces anchor the NCs to the supports as the solvent sublimes away during freeze-drying. The immobilized NCs facilitate the washing of these solids to remove or replace surface ligands without causing NC leaching or aggregation, as discussed in more detail below.

https://dx.doi.org/10.1021/acs.chemmater.0c03615
Chem. Mater. XXXX, XXX, XXX−XXX

Optical absorbance spectra of 1% NCs on MCC and TiO_2 determined using an integrating sphere are shown in Figure 1d (see the Experimental Methods section). The spectra are normalized at a wavelength of 420 nm to roughly equalize the volume of gold in each spectrum[54,55] and emphasize differences in the energy, intensity, and line width of the localized surface plasmon resonance (LSPR) compared to the LSPR of the dispersed NCs (dashed spectrum in Figure 1d). The spectra were fit to the following expression

$$\mathrm{Abs}(E) = \frac{c_0}{\pi}\frac{\gamma_0/2}{(E-E_0)^2 + (\gamma_0/2)^2} + \frac{c_1}{1+e^{-\left(\frac{E-E_1}{\gamma_1}\right)}} + \frac{c_2}{1+e^{-\left(\frac{E-E_2}{\gamma_2}\right)}} \quad (1)$$

consisting of a Lorentzian LSPR with peak energy E_0 and line width (FWHM) γ_0 and sp ← d interband transitions (ITs) described by switching functions at E_1 = 2.4 eV (visible IT) and E_2 = 3.4 eV (UV IT) with transition widths γ_1 and γ_2, respectively.[56,57] The NC colloid has a single-component Lorentzian LSPR with E_0 = 2.37 eV and γ_0 = 0.32 eV. The LSPR of the NCs supported on MCC and TiO_2 is also reasonably well fit by a single Lorentzian peak, but the peak is red-shifted and broadened compared to the LSPR of the NCs in solution (Figure S12 and Table S1). We attribute this red shifting and broadening primarily to (i) the larger dielectric constant of the environment of the supported NCs[58−60] (the real part of the dielectric constants of water, cellulose, and TiO_2 at 520 nm are 1.78, 2.17,[61] and ∼8,[62,63] respectively), (ii) the more heterogeneous dielectric environment of the supported NCs, and (iii) electromagnetic coupling between some of the supported NCs in each sample. Absorbance tails in the red (<2 eV) are caused by a small population of clustered NCs on each support, which are visible in the TEM images (Figure 1b,c). The shoulder at ∼1.8 eV in the NC/MCC spectrum may indicate a greater number of strongly coupled NCs on MCC than on TiO_2, possibly due to a larger number of small NC clusters (i.e., dimers and trimers) that form on the large, sheetlike, low-surface-area MCC particles (see Figures 1b and S3). The absorbance tail at >3 eV (<415 nm) in the NC/TiO_2 spectrum results from light absorption by TiO_2.

Figure 2 shows images and spectra of NC/MCC samples with NC loadings of 1, 5, and 20 wt %. With increasing NC loading, the sample color changes from mauve to deep violet and then nearly black (Figure 2a−c). TEM images show that the NCs remain well dispersed but form an increasing number of small NC clusters at higher NC loading. The normalized absorbance spectra (Figure 2d) show a progressive weakening of the LSPR of the isolated NCs (at 2.35−2.4 eV) and growing absorption at lower energies as a result of increased inter-NC optical coupling due to the higher NC density and more prevalent clustering. The high-energy LSPR decreases in intensity because there are fewer isolated NCs and more clusters that lack strong plasmon modes at this energy (e.g., nonlinear trimers and larger aggregates). At the same time, NC coupling and clustering produce a multitude of new plasmon modes at low energy, eventually resulting in strong panchromatic absorption across the visible and near-infrared spectrum that yields a black material at 20% NC loading.

The extent of NC clustering on MCC and TiO_2 could be reduced by adding trisodium citrate to the slurries prior to freeze-drying. As an anionic ligand, citrate can enhance inter-NC electrostatic repulsion[64] and thereby reduce the tendency

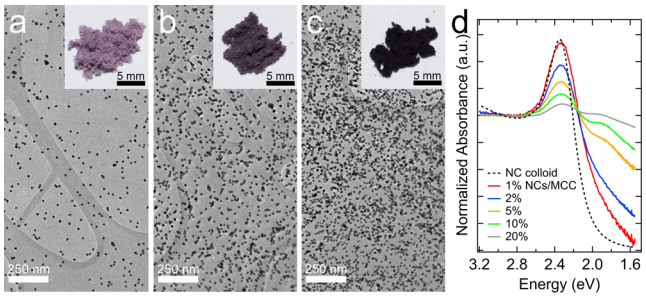

Figure 2. NC/MCC powders as a function of NC loading. TEM images and photographs of samples with (a) 1 wt %, (b) 5 wt %, and (c) 20 wt % NC loading. Higher NC loading results in more NC clustering. Some of the NCs within the clusters appear to have fused together into larger NCs, probably as a result of electron beam heating. (d) Optical absorbance spectra of dried layers of NC/MCC samples with 1, 2, 5, 10, and 20 wt % NCs compared to a spectrum of the aqueous dispersion of the NCs. The spectra are normalized for total gold volume at λ = 420 nm. All samples were prepared without added citrate. See Figure S13 for photographs of MCC samples with 0−20 wt % NCs.

for NCs to aggregate during the freeze-drying process. Citrate adsorption also reduced the aggregation of the support particles. Figure 3 compares photographs, absorbance spectra, and TEM images of NC/MCC and NC/TiO_2 samples (1% NC loading) made with 0 versus 2.5 mM citrate. Citrate addition changes the color of the powders from mauve (for MCC) or violet (for TiO_2) to red−violet, much closer to the color of the colloidal NC dispersion. The optical spectra show decreased absorption at low energy and narrower LSPRs, consistent with less NC clustering in the citrate-spiked samples. TEM images verified that the number and size of the NC clusters are reduced upon citrate addition. The effect of citrate increased with citrate concentration and was larger for (i) 5% than 1% NC loading and (ii) TiO_2 than MCC supports because NC clustering and support particle aggregation are more significant in such samples (Figure S14).

Importantly, the added citrate was easily removed after freeze-drying by rinsing the supported NCs with water at room temperature to yield cleaner NC surfaces.[25] Attenuated total reflectance Fourier transform infrared (ATR-FTIR) spectra show that water rinsing (solvent extraction) lowers the citrate concentration below the instrument detection limit (Figure S15). Moreover, the color of the rinsed samples was unchanged, indicating that citrate removal was achieved without causing significant NC clustering. A major advantage of using a charged, weakly bound, and soluble ligand like citrate is that it can be added to tune the degree of NC clustering on the support and then removed with a mild treatment (such as rinsing in water at room temperature) to expose the NC surfaces for catalysis.

We used solution-phase reductive deposition of platinum to establish that the supported NCs are catalytically active. In these experiments, NC/MCC powders prepared without added citrate were suspended in water and heated in the presence of H_2PtCl_6 and 10% methanol (a reducing agent) at 65 °C in the dark (see the Experimental Methods section). Similar chemistries have been previously used to grow Pt on other Au nanostructures.[65−68] TEM images show the selective growth of Pt nodules on the gold NCs, with no Pt detected on the cellulose support (Figure 4). Analysis of several images indicates that at least 95% of the NCs had Pt nodules after 6 h

https://dx.doi.org/10.1021/acs.chemmater.0c03615
Chem. Mater. XXXX, XXX, XXX−XXX

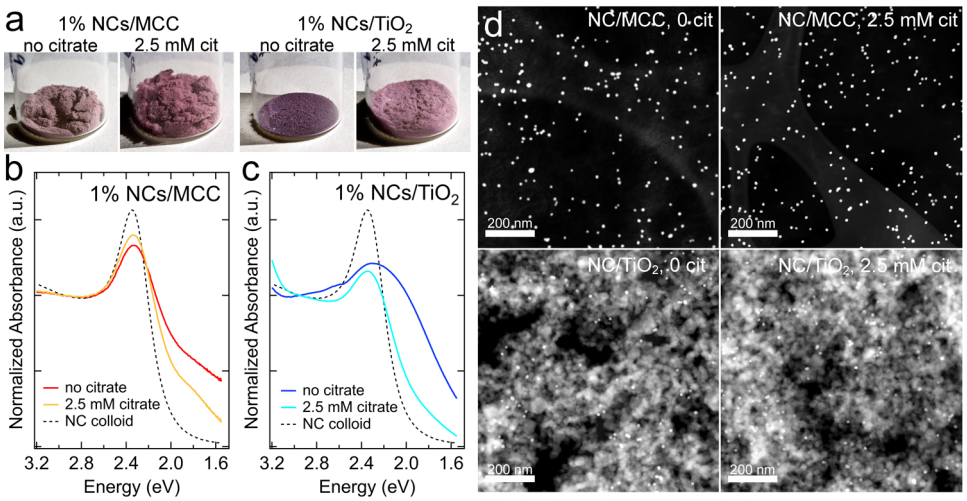

Figure 3. Effect of citrate addition on Au NC clustering and support porosity. (a) Photographs, (b, c) absorbance spectra, and (d) representative dark-field STEM images of 1% NC/MCC and NC/TiO_2 samples made with 0 or 2.5 mM citrate. The spectrum of an aqueous dispersion of the NCs is also shown. All spectra are normalized at λ = 420 nm.

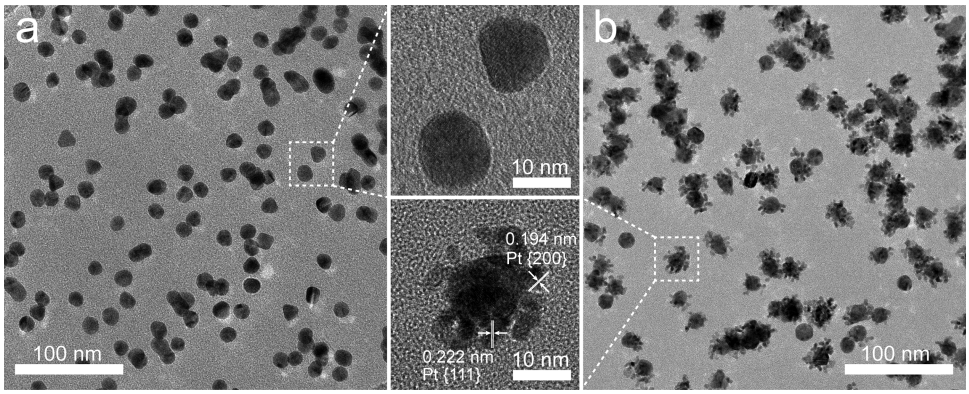

Figure 4. Platinum deposition on the supported NCs. TEM images (a) before and (b) after heating a NC/MCC suspension (5 wt % NCs) with H_2PtCl_6 in a 10:90 methanol–water mixture at 65 °C for 6 h in the dark. Magnified images of several of the NCs are also shown. The measured spacing of the lattice fringes indicates that the nodules are crystalline Pt.

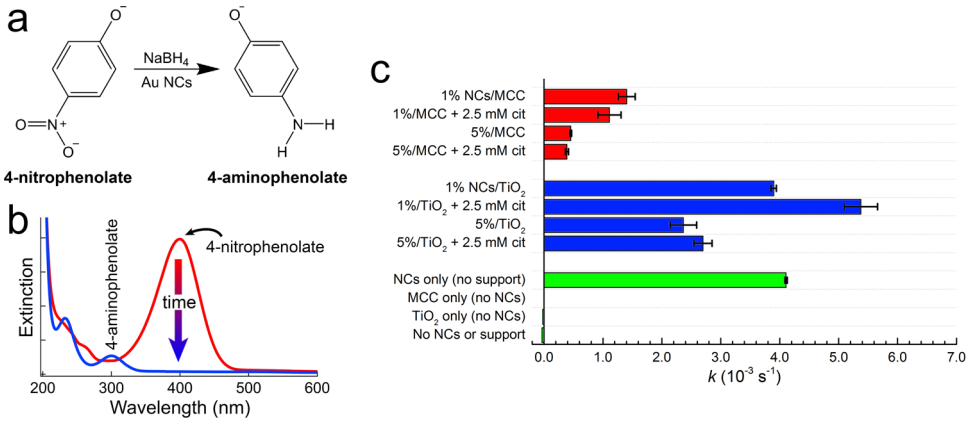

Figure 5. Catalyzed reduction of 4-nitrophenol by Au NCs. (a) Reaction scheme for the reduction of 4-nitrophenolate to 4-aminophenolate by sodium borohydride on the surface of Au NCs. (b) Solution extinction spectra before and after 4-nitrophenolate reduction. Reaction kinetics were monitored via the decay of the nitrophenolate absorbance peak at 400 nm. (c) Pseudo-first-order rate constants for the reduction reaction carried out in excess $NaBH_4$ for suspensions of NC/MCC (red bars) or NC/TiO_2 (blue bars) with 1 or 5% NC loading and 0 or 2.5 mM citrate added prior to freeze-drying. These powders were resuspended without washing off the added citrate. Also shown are data for colloidal (unsupported) NC samples without added citrate and several negative control experiments without NCs (green bars). All samples contained the same concentrations of 4-nitrophenol and $NaBH_4$, and all samples with NCs contained the same mass of NCs (1 μg/mL). Error bars denote the standard deviation of three measurements. See Figure S17 for raw data and fits.

https://dx.doi.org/10.1021/acs.chemmater.0c03615
Chem. Mater. XXXX, XXX, XXX−XXX

of reaction. In contrast, no Pt deposition was observed in the absence of methanol (Figure S16) because methanol is the sacrificial electron donor needed to sustain the reduction of Pt on the NC surface. In control reactions without NCs, Pt deposition was evident only in a few areas of the MCC, indicating that Pt deposition is mediated by the Au surface. The deposition of Pt onto the supported gold NCs shows that the NCs are in contact with the surrounding solution and not blocked by the cellulose support or residual citrate ligands.

To better understand the catalytic activity of the freeze-dried supported NCs, we measured their ability to catalyze the solution-phase reduction of 4-nitrophenol to 4-aminophenol by sodium borohydride (Figure 5a). This is a well-known model reaction that can be conveniently monitored via optical extinction spectroscopy by measuring the decay of the 4-nitrophenolate absorption peak at 400 nm (Figure 5b).[69] In our experiments, aqueous 4-nitrophenol was added to a suspension of the supported NCs in aqueous $NaBH_4$ and the extinction at 400 nm was measured in situ with constant stirring at 15 °C (see the Experimental Methods section). Measurements were conducted in triplicate on samples with 1 or 5% NC loading on MCC or TiO_2 at equal total concentrations of NCs (1 μg/mL), $NaBH_4$, and 4-nitrophenol (with $[NaBH_4]/[4\text{-nitrophenol}] = 150$). Pseudo-first-order rate constants extracted from fits of the resulting 4-nitrophenolate concentration versus time data are shown in Figure 5c. We found that NC/MCC and NC/TiO_2 samples catalyze nitrophenol reduction at different rates, with the reaction proceeding significantly faster on TiO_2 than on MCC. We attribute the larger rate constants on TiO_2 to (i) favorable metal−support interactions for Au/TiO_2,[70−72] (ii) the smaller size of the TiO_2 particles, which is expected to allow freer diffusion of molecular reactants and products compared to the larger, more aggregated, and occluded MCC particles (see Figure S3), and (iii) reduced NC clustering on the larger-surface-area TiO_2 support (51 m^2/g versus 7 m^2/g for MCC). The NC/TiO_2 samples with 1% NC loading had about the same rate constant as the unsupported NC colloid, confirming the existence of a cooperative NC/TiO_2 effect that counterbalances the reduction in NC surface area due to adsorption on the support. Increasing the NC loading to 5% resulted in smaller rate constants on both supports, probably due to increased NC clustering, occlusion, and competition between the NCs for 4-nitrophenol. Citrate addition had an insignificant effect on the rates except in the case of 1% NCs/TiO_2 samples, where it resulted in a 30% larger rate constant, likely by suppressing NC cluster formation. Overall, these experiments demonstrate that the supported NCs are catalytically active and that the rate of this model reaction depends strongly on the support material and NC loading.

Thermal stability is an important requirement for practical supported metal NC catalysts, especially plasmonic photocatalysts. We investigated the bulk thermal stability of NC/MCC and NC/TiO_2 samples by thermogravimetric analysis (TGA) in an inert atmosphere (nitrogen) from room temperature to 500 °C. For NC/MCC samples without added citrate, pyrolysis of the support began at ∼225 °C and was largely complete by ∼350 °C, leaving a black residue of carbon and gold (Figure 6a,c). NC/MCC samples containing ∼6 wt % sodium citrate showed slightly greater total mass loss but over a significantly wider temperature range (175−450 °C). Thus, citrate should be removed from NC/MCC catalysts not only to boost NC catalytic activity but also to avoid

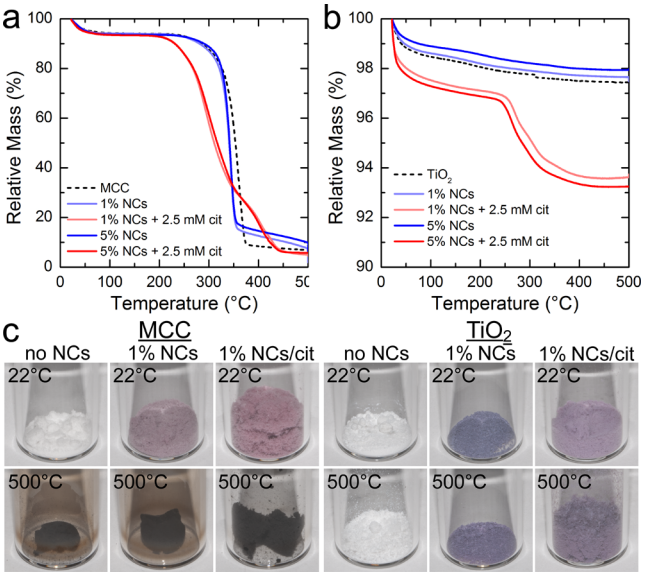

Figure 6. Thermogravimetric analysis of the supported NCs. (a) TGA traces for NC/MCC samples (1 or 5% NCs with or without 2.5 mM citrate) in flowing nitrogen. Data for pure MCC are also shown. The initial mass loss (up to ∼200 °C) is caused by water desorption. MCC and citrate pyrolysis occurred above ∼200 °C. (b) Corresponding data for NC/TiO_2 samples and pure TiO_2. The citrate-spiked samples showed greater water loss below 200 °C (from citrate hydrates) and citrate pyrolysis above ∼250 °C. (c) Photographs of NC/MCC and NC/TiO_2 samples (1% NCs with and without citrate) before and after annealing at 500 °C in nitrogen for 15 min in a tube furnace. Photos of pure MCC and TiO_2 are also shown for reference. See Figure S18 for TEM images of one of the NC/TiO_2 samples after the 500 °C anneal.

degrading the already low thermal stability of MCC. In contrast, NC/TiO_2 samples showed only small mass losses (primarily due to dehydration and citrate pyrolysis), while the color of these materials changed from mauve to violet as a result of very minor NC size and shape changes at the elevated temperature (Figures 6b,c and S18).

Finally, we show that freeze-drying can be scaled to larger batch sizes and extended to other types of metal NCs, making it an attractive general method for preparing supported NC catalysts. As a demonstration, we increased the batch size from 0.1 to 1 g of 1% NC/MCC and NC/TiO_2 and obtained products identical in color and microstructure to those shown in Figure 1 (Figure S19). Further increases in batch size are possible by employing larger lyophilizers. We also used freeze-drying to deposit triangular Au nanoprisms (55−60 nm edge length and capped with CTAC, see the Experimental Methods section) on MCC and TiO_2 supports (Figure 7). As with the spheroidal Au NCs, the supported nanoprisms were well dispersed and retained their original shape and colloidal color (blue in this case). The presence of CTAC had no obvious impact on the freeze-drying process. Absorbance spectra of the supported nanoprisms show weaker, broader, and slightly blue-shifted LSPRs compared to the colloidal (unsupported) nanoprisms, which may reflect some blunting/rounding of the prism corners during freeze-drying or sample preparation.[58] The exact cause of these spectral changes is the subject of ongoing investigations in our laboratory.

https://dx.doi.org/10.1021/acs.chemmater.0c03615
Chem. Mater. XXXX, XXX, XXX−XXX

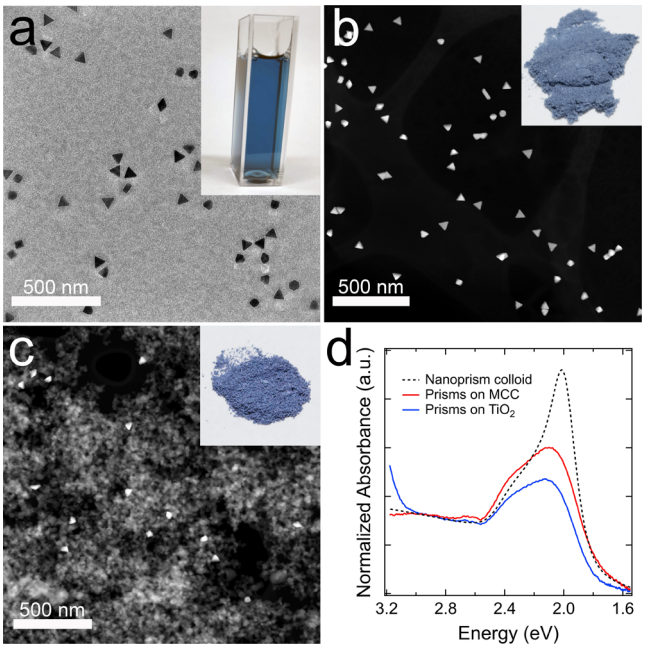

Figure 7. Supported Au nanoprisms made by freeze-drying. (a) TEM image and a photograph of the colloidal Au nanoprisms. (b) Dark-field STEM image and a photograph of the nanoprisms on MCC (~0.6 wt %). (c) Corresponding data for nanoprisms on TiO_2 (~0.6 wt %). (d) Absorbance spectra of the supported and colloidal nanoprisms. All spectra are normalized at λ = 420 nm.

CONCLUSIONS

This paper demonstrates that slurry freeze-drying is a simple, mild, reproducible, and scalable method to load premade colloidal gold nanocrystals onto organic and inorganic supports to obtain uniform NC dispersion with tunable NC loading (to at least 20 wt %) and retention of original NC size and shape. We showed that sodium citrate suppresses the clustering of gold NCs on cellulose and TiO_2 and can be subsequently rinsed away to yield supported NCs with cleaner surfaces, avoiding the need for high-temperature calcination that can degrade NC monodispersity. Two model reactions were used to establish the catalytic activity of the supported NCs in water. The generality of the method was demonstrated by depositing (i) 12−14 nm diameter Au NCs onto SiO_2 and carbon, (ii) ~3.5 nm diameter Au NCs onto MCC and TiO_2, and (iii) triangular Au nanoprisms onto cellulose and TiO_2. Due to its many advantages, slurry freeze-drying should prove useful for making a wide variety of uniform supported NC catalysts from chemically synthesized colloidal NCs. We expect that the freeze-drying of colloidal mixtures can be extended beyond metal NCs to load many other types of colloids (inorganic NCs, organic nanoparticles, nanowires, etc.) onto a wide variety of support materials (carbon, metal oxides, polymers, etc.) for applications in catalysis, energy conversion and storage, optoelectronics, and sensing.

ASSOCIATED CONTENT

Supporting Information

The Supporting Information is available free of charge at https://pubs.acs.org/doi/10.1021/acs.chemmater.0c03615.

Experimental results include FTIR, XRD, TEM, SEM and TGA data, photographs, and raw spectral data and fits (PDF)

AUTHOR INFORMATION

Corresponding Author

Matt Law − *Department of Chemistry, Department of Materials Science and Engineering, and Department of Chemical and Biomolecular Engineering, University of California, Irvine, Irvine, California 92697, United States;* orcid.org/0000-0001-7645-9908; Email: lawm@uci.edu.

Author

Andy Y. Yang − *Department of Chemistry, University of California, Irvine, Irvine, California 92697, United States*

Complete contact information is available at: https://pubs.acs.org/10.1021/acs.chemmater.0c03615

Author Contributions

A.Y.Y. carried out all experiments. M.L. directed the research. Both authors analyzed the data and wrote the manuscript. Both authors have given approval to the final version of the manuscript.

Notes

The authors declare no competing financial interest.

ACKNOWLEDGMENTS

This work was supported by the National Science Foundation Center for Chemical Innovation on Chemistry at the Space-Time Limit (CaSTL), Grant Number CHE-1414466. Materials characterization was performed at the user facilities of the UC Irvine Materials Research Institute (IMRI).

REFERENCES

(1) Jia, C.-J.; Schüth, F. Colloidal metal nanoparticles as a component of designed catalyst. *Phys. Chem. Chem. Phys.* **2011**, *13*, 2457−2487.

(2) Munnik, P.; de Jongh, P. E.; de Jong, K. P. Recent developments in the synthesis of supported catalysts. *Chem. Rev.* **2015**, *115*, 6687−6718.

(3) Corma, A.; Garcia, H. Supported gold nanoparticles as catalysts for organic reactions. *Chem. Soc. Rev.* **2008**, *37*, 2096−2126.

(4) Ma, Z.; Dai, S. Design of novel structured gold nanocatalysts. *ACS Catal.* **2011**, *1*, 805−818.

(5) Stratakis, M.; Garcia, H. Catalysis by supported gold nanoparticles: Beyond aerobic oxidative processes. *Chem. Rev.* **2012**, *112*, 4469−4506.

(6) Nakamura, T.; Yamada, Y.; Yano, K. Direct synthesis of monodispersed thiol-functionalized nanoporous silica spheres and their application to a colloidal crystal embedded with gold nanoparticles. *J. Mater. Chem.* **2007**, *17*, 3726−3732.

(7) Haruta, M.; Yamada, N.; Kobayashi, T.; Iijima, S. Gold catalysts prepared by coprecipitation for low-temperature oxidation of hydrogen and of carbon monoxide. *J. Catal.* **1989**, *115*, 301−309.

(8) Tsubota, S.; Cunningham, D. A. H.; Bando, Y.; Haruta, M. Preparation of nanometer gold strongly interacted with TiO_2 and the structure sensitivity in low-temperature oxidation of CO. *Stud. Surf. Sci. Catal.* **1995**, *91*, 227−235.

(9) Bitter, J. H.; van der Lee, M. K.; Slotboom, A. G. T.; van Dillen, A. J.; de Jong, K. P. Synthesis of highly loaded highly dispersed nickel on carbon nanofibers by homogeneous deposition-precipitation. *Catal. Lett.* **2003**, *89*, 139−142.

(10) Haruta, M. Size- and support-dependency in the catalysis of gold. *Catal. Today* **1997**, *36*, 153−166.

(11) Liu, X.; Glasser, B.; Khinast, J. In *Impact of Impregnation and Drying on the Metal Distribution in Supported Catalysts*, 2007 AIChE Annual Meeting; 2007; pp 4473−4487.

(12) Mondloch, J. E.; Bayram, E.; Finke, R. G. A review of the kinetics and mechanisms of formation of supported-nanoparticle heterogeneous catalysts. *J. Mol. Catal., A* **2012**, *355*, 1−38.
(13) Grunwaldt, J.-D.; Kiener, C.; Wögerbauer, C.; Baiker, A. Preparation of supported gold catalysts for low-temperature CO oxidation via "size-controlled" gold colloids. *J. Catal.* **1999**, *181*, 223−232.
(14) Prati, L.; Martra, G. New gold catalysts for liquid phase oxidation. *Gold Bull.* **1999**, *32*, 96−101.
(15) Porta, F.; Prati, L.; Rossi, M.; Coluccia, S.; Martra, G. Metal sols as a useful tool for heterogeneous gold catalyst preparation: Reinvestigation of a liquid phase oxidation. *Catal. Today* **2000**, *61*, 165−172.
(16) Tai, Y.; Watanabe, M.; Kaneko, K.; Tanemura, S.; Miki, T.; Murakami, J.; Tariji, K. Preparation of gold cluster/silica nanocomposite aerogel via spontaneous wet-gel formation. *Adv. Mater.* **2001**, *13*, 1611−1614.
(17) Tai, Y.; Murakami, J.; Tajiri, K.; Ohashi, F.; Daté, M.; Tsubota, S. Oxidation of carbon monoxide on Au nanoparticles in titania and titania-coated silica aerogels. *Appl. Catal., A* **2004**, *268*, 183−187.
(18) Comotti, M.; Li, W. C.; Spliethoff, B.; Schüth, F. Support effect in high activity gold catalysts for CO oxidation. *J. Am. Chem. Soc.* **2006**, *128*, 917−924.
(19) Chou, J.; McFarland, E. W. Direct propylene epoxidation on chemically reduced Au nanoparticles supported on titania. *Chem. Commun.* **2004**, 1648−1649.
(20) Lee, I.; Morales, R.; Albiter, M. A.; Zaera, F. Synthesis of heterogeneous catalysts with well shaped platinum particles to control reaction selectivity. *Proc. Natl. Acad. Sci. U.S.A.* **2008**, *105*, 15241−15246.
(21) Rossi, L. M.; Fiorio, J. L.; Garcia, M. A. S.; Ferraz, C. P. The role and fate of capping ligands in colloidally prepared metal nanoparticle catalysts. *Dalton Trans.* **2018**, *47*, 5889−5915.
(22) Biella, S.; Porta, F.; Prati, L.; Rossi, M. Surfactant-protected gold particles: new challenge for gold-on-carbon catalysts. *Catal. Lett.* **2003**, *90*, 23−29.
(23) Pietron, J. J.; Stroud, R. M.; Rolison, D. R. Using three dimensions in catalytic mesoporous nanoarchitectures. *Nano Lett.* **2002**, *2*, 545−549.
(24) Zheng, N.; Stucky, G. D. A general synthetic strategy for oxide-supported metal nanoparticle catalysts. *J. Am. Chem. Soc.* **2006**, *128*, 14278−14280.
(25) Lopez-Sanchez, J. A.; Dimitratos, N.; Hammond, C.; Brett, G. L.; Kesavan, L.; White, S.; Miedziak, P.; Tiruvalam, R.; Jenkins, R. L.; Carley, A. F.; Knight, D.; Kiely, C. J.; Hutchings, G. J. Facile removal of stabilizer-ligands from supported gold nanoparticles. *Nat. Chem.* **2011**, *3*, 551−556.
(26) Morris, C. A.; Anderson, M. L.; Stroud, R. M.; Merzbacher, C. I.; Rolison, D. R. Silica sol as a nanoglue: Flexible synthesis of composite aerogels. *Science* **1999**, *284*, 622−624.
(27) Kónya, Z.; Puntes, V. F.; Kiricsi, I.; Zhu, J.; Ager, J. W., III; Ko, M. K.; Frei, H.; Alivisatos, P.; Somorjai, G. A. Synthetic insertion of gold nanoparticles into mesoporous silica. *Chem. Mater.* **2003**, *15*, 1242−1248.
(28) Rioux, R. M.; Song, H.; Hoefelmeyer, J. D.; Yang, P.; Somorjai, G. A. High-Surface-area catalyst design: Synthesis, characterization, and reaction studies of platinum nanoparticles in mesoporous SBA-15 silica. *J. Phys. Chem. B* **2005**, *109*, 2192−2202.
(29) Song, H.; Rioux, R. M.; Hoefelmeyer, J. D.; Komor, R.; Niesz, K.; Grass, M.; Yang, P.; Somorjai, G. A. Hydrothermal growth of mesoporous SBA-15 silica in the presence of PVP-stabilized Pt nanoparticles: Synthesis, characterization, and catalytic properties. *J. Am. Chem. Soc.* **2006**, *128*, 3027−3037.
(30) Zhang, Y.; He, S.; Guo, W.; Hu, Y.; Huang, J.; Mulcahy, J. R.; Wei, W. D. Surface-plasmon-driven hot electron photochemistry. *Chem. Rev.* **2018**, *118*, 2927−2954.
(31) Kosmulski, M. The pH dependent surface charging and points of zero charge. VI. Update. *J. Colloid Interface Sci.* **2014**, *426*, 209−212.
(32) Xu, Y.; Cao, Q.; Svec, F.; Fréchet, J. M. J. Porous polymer monolithic column with surface-bound gold nanoparticles for the capture and separation of cysteine-containing peptides. *Anal. Chem.* **2010**, *82*, 3352−3358.
(33) Cao, Y.; Lv, M.; Xu, H.; Svec, F.; Tan, T.; Lv, Y. Planar monolithic porous polymer layers functionalized with gold nanoparticles as large-area substrates for sensitive surface-enhanced Raman scattering sensing of bacteria. *Anal. Chim. Acta* **2015**, *896*, 111−119.
(34) Yang, J.; Guo, Y.; Jiang, R.; Qin, F.; Zhang, H.; Lu, W.; Wang, J.; Yu, J. C. High-efficiency "Working-in-Tandem" nitrogen photofixation achieved by assembling plasmonic gold nanocrystals on ultrathin titania nanosheets. *J. Am. Chem. Soc.* **2018**, *140*, 8497−8508.
(35) Hua, T.-C.; Liu, B.-L.; Zhang, H. *Freeze-Drying of Pharmaceutical and Food Products*; Woodhead Publishing Limited: Cambridge, 2010.
(36) Lévy, R.; Thanh, N. T. K.; Doty, R. C.; Hussain, I.; Nichols, R. J.; Schiffrin, D. J.; Brust, M.; Fernig, D. G. Rational and combinatorial design of peptide capping ligands for gold nanoparticles. *J. Am. Chem. Soc.* **2004**, *126*, 10076−10084.
(37) Abdelwahed, W.; Degobert, G.; Stainmesse, S.; Fessi, H. Freeze drying of nanoparticles: formulation, process and storage considerations. *Adv. Drug Delivery Rev.* **2006**, *58*, 1688−1713.
(38) Zhang, L.; Li, P.; Li, D.; Guo, S.; Wang, E. Effect of freeze-thawing on lipid bilayer-protected gold nanoparticles. *Langmuir* **2008**, *24*, 3407−3411.
(39) Khlebtsov, B. N.; Panfilova, E. V.; Terentyuk, G. S.; Maksimova, I. L.; Ivanov, A. V.; Khlebtsov, N. G. Plasmonic nanopowders for photothermal therapy of tumors. *Langmuir* **2012**, *28*, 8994−9002.
(40) Alkilany, A. M.; Abulateefeh, S. R.; Mills, K. K.; Bani Yaseen, A. I.; Hamaly, M. A.; Alkhatib, H. S.; Aiedeh, K. M.; Stone, J. W. Colloidal stability of citrate and mercaptoacetic acid capped gold nanoparticles upon lyophilization: Effect of capping ligand attachment and type of cryoprotectants. *Langmuir* **2014**, *30*, 13799−13808.
(41) Gupta, A.; Moyano, D. F.; Parnsubsakul, A.; Papadopoulos, A.; Wang, L. S.; Landis, R. F.; Das, R.; Rotello, V. M. Ultrastable and biofunctionalizable gold nanoparticles. *ACS Appl. Mater. Interfaces* **2016**, *8*, 14096−14101.
(42) Vergunst, T.; Kapteijn, F.; Moulijn, J. A. Monolithic catalysts - non-uniform active phase distribution by impregnation. *Appl. Catal., A* **2001**, *213*, 179−187.
(43) Xi, X. L.; Nie, Z. R.; Jiang, Y. B.; Xu, X. Y.; Zuo, T. Y. Preparation and characterization of ultrafine cobalt powders and supported cobalt catalysts by freeze drying. *Powder Technol.* **2009**, *191*, 107−110.
(44) Eggenhuisen, T. M.; Friedrich, H.; Nudelman, F.; Zečević, J.; Sommerdijk, N. A. J. M.; de Jongh, P. E.; de Jong, K. P. Controlling the distribution of supported nanoparticles by aqueous synthesis. *Chem. Mater.* **2013**, *25*, 890−896.
(45) Vilé, G.; Baudouin, D.; Remediakis, I. N.; Copéret, C.; López, N.; Pérez-Ramírez, J. Silver nanoparticles for olefin production: New insights into the mechanistic description of propyne hydrogenation. *ChemCatChem* **2013**, *5*, 3750−3759.
(46) Eggenhuisen, T. M.; Munnik, P.; Talsma, H.; de Jongh, P. E.; de Jong, K. P. Freeze-drying for controlled nanoparticle distribution in Co/SiO_2 Fischer-Tropsch catalysts. *J. Catal.* **2013**, *297*, 306−313.
(47) Kim, H. J.; Choi, S. M.; Nam, S. H.; Seo, M. H.; Kim, W. B. Effect of Rh content on carbon-supported PtRh catalysts for dehydrogenative electrooxidation of cyclohexane to benzene over polymer electrolyte membrane fuel cell. *Appl. Catal., A* **2009**, *352*, 145−151.
(48) Kim, H. J.; Choi, S. M.; Green, S.; Tompsett, G. A.; Lee, S. H.; Huber, G. W.; Kim, W. B. Highly active and stable PtRuSn/C catalyst for electrooxidations of ethylene glycol and glycerol. *Appl. Catal., B* **2011**, *101*, 366−375.
(49) Bastús, N. G.; Comenge, J.; Puntes, V. Kinetically controlled seeded growth synthesis of citrate-stabilized gold nanoparticles of up to 200 nm: Size focusing versus Ostwald ripening. *Langmuir* **2011**, *27*, 11098−11105.

https://dx.doi.org/10.1021/acs.chemmater.0c03615
Chem. Mater. XXXX, XXX, XXX−XXX

(50) Johnsen, E.; Bradtzaeg, O. K.; Vehus, T.; Roberg-Larsen, H.; Bogoeva, V.; Ademi, O.; Hildahl, J.; Lundanes, E.; Wilson, S. R. A critical evaluation of Amicon Ultra centrifugal filters for separating proteins, drugs and nanoparticles in biosamples. *J. Pharm. Biomed. Anal.* **2016**, *120*, 106−111.
(51) Scarabelli, L.; Coronado-Puchau, M.; Giner-Casares, J. J.; Langer, J.; Liz-Marzán, L. M. Monodisperse gold nanotriangles: Size control, large-scale self-assembly, and performance in surface-enhanced Raman scattering. *ACS Nano* **2014**, *8*, 5833−5842.
(52) Luan, Z.; Salk, T.; Abelson, A.; Jean, S.; Law, M. Reversible aggregation of covalently cross-linked gold nanocrystals by linker oxidation. *J. Phys. Chem. C* **2019**, *123*, 23643−23654.
(53) Sweeney, S. F.; Woehrle, G. H.; Hutchison, J. E. Rapid purification and size separation of gold nanoparticles via diafiltration. *J. Am. Chem. Soc.* **2006**, *128*, 3190−3197.
(54) Rodríguez-Fernández, J.; Pérez-Juste, J.; Mulvaney, P.; Liz-Marzán, L. M. Spatially-directed oxidation of gold nanoparticles by Au(III)-CTAB complexes. *J. Phys. Chem. B* **2005**, *109*, 14257−14261.
(55) Scarabelli, L.; Grzelczak, M.; Liz-Marzán, L. M. Tuning gold nanorod synthesis through prereduction with salicylic acid. *Chem. Mater.* **2013**, *25*, 4232−4238.
(56) Engelbrekt, C.; Crampton, K. T.; Fishman, D. A.; Law, M.; Apkarian, V. A. Efficient plasmon-mediated energy funneling to the surface of Au@Pt core-shell nanocrystals. *ACS Nano* **2020**, *14*, 5061−5074.
(57) Etchegoin, P. G.; Le Ru, E. C.; Meyer, M. An analytic model for the optical properties of gold. *J. Chem. Phys.* **2006**, *125*, No. 164705.
(58) Kelly, K. L.; Coronado, E.; Zhao, L. L.; Schatz, G. C. The optical properties of metal nanoparticles: The influence of size, shape, and dielectric environment. *J. Phys. Chem. B* **2003**, *107*, 668−677.
(59) Chen, H.; Kou, X.; Yang, Z.; Ni, W.; Wang, J. Shape- and size-dependent refractive index sensitivity of gold nanoparticles. *Langmuir* **2008**, *24*, 5233−5237.
(60) Jeon, H. B.; Tsalu, P. V.; Ha, J. W. Shape effect on the refractive index sensitivity at localized surface plasmon resonance inflection points of single gold nanocubes with vertices. *Sci. Rep.* **2019**, *9*, No. 13635.
(61) Kasarova, S.; Sultanova, N.; Ivanov, C.; Nikolov, I. Analysis of the dispersion of optical plastic materials. *Opt. Mater.* **2007**, *29*, 1481−1490.
(62) DeVore, J. R. Refractive indices of rutile and sphalerite. *J. Opt. Soc. Am.* **1951**, *41*, 416−419.
(63) Bendavid, A.; Martin, P. J.; Jamting, Å.; Takikawa, H. Structural and optical properties of titanium oxide thin films deposited by filtered arc deposition. *Thin Solid Films* **1999**, *355*−*356*, 6−11.
(64) Heuer-Jungemann, A.; Feliu, N.; Bakaimi, I.; Hamaly, M.; Alkilany, A.; Chakraborty, I.; Masood, A.; Casula, M. F.; Kostopoulou, A.; Oh, E.; Susumu, K.; Stewart, M. H.; Medintz, I. L.; Stratakis, E.; Parak, W. J.; Kanaras, A. G. The role of ligands in the chemical synthesis and applications of inorganic nanoparticles. *Chem. Rev.* **2019**, *119*, 4819−4880.
(65) Grzelczak, M.; Pérez-Juste, J.; García de Abajo, F. J.; Liz-Marzán, L. M. Optical properties of platinum-coated gold nanorods. *J. Phys. Chem. C* **2007**, *111*, 6183−6188.
(66) Straney, P. J.; Marbella, L. E.; Andolina, C. M.; Nuhfer, N. T.; Millstone, J. E. Decoupling mechanisms of platinum deposition on colloidal gold nanoparticle substrates. *J. Am. Chem. Soc.* **2014**, *136*, 7873−7876.
(67) Gilroy, K. D.; Ruditskiy, A.; Peng, H.-C.; Qin, D.; Xia, Y. Bimetallic nanocrystals: Syntheses, properties, and applications. *Chem. Rev.* **2016**, *116*, 10414−10472.
(68) Ortiz, N.; Zoellner, B.; Hong, S. J.; Ji, Y.; Wang, T.; Liu, Y.; Maggard, P. A.; Wang, G. Harnessing hot electrons from near IR light for hydrogen production using Pt-end-capped-AuNRs. *ACS Appl. Mater. Interfaces* **2017**, *9*, 25962−25969.
(69) Hervés, P.; Pérez-Lorenzo, M.; Liz-Marzán, L. M.; Dzubiella, J.; Lu, Y.; Ballauff, M. Catalysis by metallic nanoparticles in aqueous solution: Model reactions. *Chem. Soc. Rev.* **2012**, *41*, 5577−5587.
(70) Wang, Y.; Widmann, D.; Behm, R. J. Influence of TiO_2 bulk defects on CO adsorption and CO oxidation on Au/TiO_2: Electronic metal-support interactions (EMSIs) in supported Au catalysts. *ACS Catal.* **2017**, *7*, 2339−2345.
(71) Tauster, S. J. Strong metal-support interactions. *Acc. Chem. Res.* **1987**, *20*, 389−394.
(72) Chakraborty, S.; Ansar, S. M.; Stroud, J. G.; Kitchens, C. L. Comparison of colloidal versus supported gold nanoparticle catalysis. *J. Phys. Chem. C* **2018**, *122*, 7749−7758.

https://dx.doi.org/10.1021/acs.chemmater.0c03615
Chem. Mater. XXXX, XXX, XXX−XXX